Supporting Information for "Simulated Impact of Time-varying River Runoff and Greenland Freshwater Discharge on Sea Level Variability in the Beaufort Gyre over 2005-2018"

S. Tajouri[1], W. Llovel[1], F. Sévellec[1,2], J.-M. Molines[3], P.Mathiot[3], T. Penduff [3], S. Leroux[4]

[1]Univ Brest, CNRS, IRD, IFREMER, Laboratoire d'Océanographie Physique et Spatiale, F-29280 Plouzané, France

[2]Odyssey team-project, INRIA CNRS, Brest, France

[3]Université Grenoble Alpes, CNRS, INRAE, IRD, Grenoble INP, Institut des Géosciences de l'Environnement, Grenoble, France

[4]Datlas, Grenoble, France

Contents of this file

1. Text S1 to S11
2. Figures S1 to S11

Introduction This supporting information includes a map to help readers locate the main Arctic Ocean features mentioned in the article (Fig. S1). It also includes a description of the set up of the model to represent Greenland and Antarctica Ice Sheets melting. Text and Fig. S2 present the location along Greenland of the discharge and indicate its nature

Corresponding author: Soumaïa Tajouri, Laboratoire d'océanographie Physique et Spatiale, UMR6523 CNRS/IFREMER/IRD/UBO Ifremer - Centre de Bretagne ZI de la Pointe du Diable, CS10070, F-29280 Plouzané, FRANCE, (soumaia.tajouri@ifremer.fr)

(surface runoff, ice shelf melting, and iceberg calving) and the depth of the grounding line of marine terminating glaciers. Text S2 also provides details about the implementation of Antarctica's freshwater fluxes.

Figs. S3 to S5 help describing the circulation in the Beaufort Gyre Region and the Arctic Ocean and how it changes between simulations. Figs. S3 and S4 show the time series of the barotropic stream function averaged in the BGR box and in the Arctic Ocean and the wind stress curl in the Beaufort Gyre Region box. Fig. S5 shows maps of the barotropic stream function mean and standard deviation over the Arctic region.

Texts and Figs. S6 and S7 complement the model assessment part of the study by showing maps of the standard deviation of the altimetry products and exp1 and maps of trends of exp1, Armitage et al., (2016) and ECCO V4r4.

Fig. S8 is showing the SLA and its decomposition into its different components for exp1 to complement the Fig. 3 of the study.

Fig. S9 shows the meridional velocity around Greenland and across a section between Greenland and Svalbard as well as barotropic transport and salinity transport across the section.

Text and Fig. S10 complement Fig. 7 of the study by showing the time series of the annual freshwater flux of GREENLAND and RIVERS.

Fig. S11 displays time-lagged correlation maps between the full column mean salinity changes at each grid point in the Arctic Ocean and the time series of SLA in the BGR box over 2005-2018.

Text S1. Fig. S1 displays a bathymetric map of the Arctic Ocean with superimposed the name of the Arctic features used in the study.

Text S2. In Greenland, the interaction between land ice and ocean (ice shelves and marine terminus) occurs in narrow fjords far from the open sea (and model limit). Therefore, we need to take into account the processes in the fjords. As there is no fjord parameterization available in NEMO, the fjords are represented in a simple way. The implementation of Greenland freshwater flux in the model is performed using surface runoffs (in kg m^{-2} s^{-1}), ice shelf melting (or subglacial runoff) (in kg m^{-2} s^{-1}), and icebergs calving rate (in Gt yr^{-1}) from Mouginot et al. (2019) and combined at some locations as shown in Fig. S2a. It is applied at the coastal model grid points closest to the 262 original points of the dataset. The ice shelf melting is implemented between the ice shelf draft at its edge and the depth of the grounding line (which corresponds to the fjord's sill depth in Greenland) which is shown on Fig. S2b. A latent heat flux is also applied at the model cells impacted by the fresh water flux from ice shelf and icebergs melting producing some cooling of these cells.

Antarctic freshwater sources are mainly driven by iceberg and ice shelf melt. Surface runoff is weak (Gilbert & Kittel, 2021) and subglacial runoff is very poorly known, not well constrained and expected to be small (Joughin et al., 2009). They are both set to 0 in this study. Iceberg melt (for both Greenland and Antactica) is explicitly represented using the lagrangian iceberg model available in NEMO (Marsh et al., 2015). In this representation, a calving rate is applied along ice shelf edges at marine terminating glaciers. When the amount of accumulated ice at a calving point reaches a pre-defined threshold, an iceberg (or a group of icebergs) is dropped into the ocean and its trajectory is computed (lagrangian approach, (Marsh et al., 2015)). The iceberg then melts during its journey, and releases fresh water along its path, until its total melting. For Antarctica, The

annual calving rate for each ice shelf is derived from Rignot, Jacobs, Mouginot, and Scheuchl (2013) and randomly spread among all the points at the ice shelf edge (Mathiot & Jourdain, 2023). Ice shelf cavities are not resolved in our simulations. Therefore the basal melt rate is prescribed at the ice shelf edge and injected at depth from the bottom of the ice shelf edge to the maximum depth of the grounding line following recommendations from Mathiot, Jenkins, Harris, and Madec (2017). The annual basal melt rate estimate per ice shelf is given by Rignot et al. (2013).

Text S3 and S4 To verify the sensitivity of the ocean circulation to the freshwater forcing variability, we calculate the barotropic stream function (as a depth-integrated volume transport) (Fig. S3) and the wind stress curl perceived by the ocean (Fig. S4) in the BGR box. Over 1980-2018, the sensitivity of the strength (mean) and the temporal variability (standard deviation) of the barotropic stream function and the wind stress curl stayed below 10% for Gr+Riv, GREENLAND, and RIVERS. It confirms that the sensitivity of the ocean circulation to freshwater flux variability is not sufficient to modulate the overall advection term. The spatial pattern of the wind stress curl sensitivities (not shown) suggests that the wind-stress curl is probably modulated via mesoscale dynamics. The opposite and quasi-compensating impacts of GREENLAND and RIVERS over the whole simulation and trends over 2005-2018 are also present in the barotropic stream function and wind stress curl time series in the BGR box. It suggests that SLA and salinity changes due to freshwater flux variability could have a feedback on the gyre circulation. A plausible mechanism for that is that the SLA variations impact the speed of the gyre changing the relative wind speed perceived by the ocean and thus the wind-stress. Fig. S3 also shows the barotropic stream function in the Arctic Ocean for each experiments and

the 3 sensitivity differences. The barotropic stream function of the whole Arctic Ocean does not vary much over 1980-2018 in the experiments nor in the sensitivity differences highlighting the consistency of the broad Arctic Ocean circulation between experiments.

Text S5. Fig. S5 displays barotropic stream function characteristics in exp1 and the sensitivity differences. In exp1, the barotropic stream function time-mean (Fig. S5a) is strong in the Eurasian basin and Nordic seas (around -10 Sv) and weaker and positive in the Canada basin. It is also weak over shallow shelves. As expected, the barotropic flow broadly follows seafloor topography. Exp1 standard deviation map shows that the variability of the barotropic stream function is greater in the deep basins than over shallow shelves (Fig. S5b). It is of around 3 Sv in the Canada basin and the Nordic seas. The barotropic streamfunction mean and standard deviation varies of the order of ± 0.5 Sv in the sensitivity differences (Fig. S5c-h). This flow variability between simulations is small compared to the magnitude of the flow but can have significant impact on the transport of salinity (as could be seen on Fig.6).

Text S6 and S7. Fig. S6 shows maps of the standard deviation (std) of the different altimetry products, exp1, and ECCO V4r4 (from annual data). Exp1 present strong standard deviations of up to 10 cm centered in the Amerasian basin with some signal in the BGR. ECCO v4r4 present similar values of std as exp1 but centered in the BGR box. Armitage et al., (2016) present lower std values in the BGR box than exp1. CCI DTU does not show a particular signal of STD in the BGR box or somewhere else in the Arctic. The Doglioni et al., (2021), CPOM, and Prandi et al., (2021) datasets have their std computed over the same period 2011-2018 and show weak std values in the BGR and the Arctic Ocean. The trends computed over similar periods in exp1, Armitage et al.,

(2016) and ECCO V4r4 display very similar spatial pattern in the BGR and the broad Arctic Ocean (Fig. S7). Therefore, exp1 is coherent with Armitage et al., (2016) and ECCO V4r4 in terms of the spatial pattern of SLA trends.

Text S8. Fig. S8 shows maps of exp1 trends over 2005-2018 of the sea level anomalies (a), the steric sea level (b), the manometric sea level (c), the halosteric sea level (d), and the thermosteric sea level (e). The mean SLA trend over 2005-2018 in the BGR box is 15.1 mm yr^{-1}. The SLA, steric and halosteric trends in exp1 are roughly twice as large as the ones of the sensitivity differences (shown in Fig. 3).

Text S9. We analyse using Fig. S9 the potential change in circulation and associated transport in the Nordic seas in the sensitivity differences. Panels a-d show the meridional velocity component averaged over the upper 500 m in exp1 and the three sensitivity differences. The colorbar is one order of magnitude smaller for the sensitivity differences than for exp1 showing the small impact of freshwater flux variability on circulation. In addition, the impact of freshwater flux variability on the meridional velocity is very similar between Gr+Riv, GREENLAND, and RIVERS. Fig. S9e show a northward coastal current in exp1 (indicated by the red box). This coastal current varies very little between simulations (Fig. S9f-h) and the associated transport of salinity is weakly impacted (Fig. S9o and p). Instead, it appears that the salinity transport across the section from Greenland to Svalbard is mainly controlled by the changed circulation along the full section (Fig. S9m and n) and little by the salinity changes (Fig. S9i-l) . Indeed, the East Greenland Current (flowing Southward and located in the middle of the section) is reduced in all sensitivity differences while the West Spitsbergen Current (northward current off Svalbard) is intensified increasing the shear between these two currents. The salin-

ity transport differences between the sensitivity differences across the section potentially impact the Arctic Ocean.

Text S10. Fig. S10 shows the annual freshwater flux time series of (a) GREENLAND and (b) RIVERS. GREENLAND discharge as a whole (black curve) increased significantly from 2000 and reached a maximum in 2012 due to abnormally high discharge from the Southwest region. RIVERS runoff exhibit high interannual variability by individual seas (grey lines) as well as by regions (pan-Arctic, North American rivers, and Eurasian rivers).

Text S11. The colored areas of maps in Fig. S11 denote regions where GREENLAND and RIVERS are having a correlation of the same sign, that is where they are having the same behavior spatially with respect to salinity changes and SLA changes. We are interested in the negative correlation in the BGR as halosteric sea level and salinity changes are anti-correlated (a decrease in salinity induces an increase in sea level). For a lag of 0 years, we expect the strong (greater than -0.8) anti-correlation in the BGR. As the time lag increases, the strong anti-correlation patch breaks spatially, decreases in size and moves northwards. From a lag of 7 years, it disappears and does not stand out from the rest of correlations that could be found in the Arctic Ocean.

References

Gilbert, E., & Kittel, C. (2021). Surface melt and runoff on antarctic ice shelves at 1.5°c, 2°c, and 4°c of future warming. *Geophysical Research Letters*, *48*(8), e2020GL091733. Retrieved from `https://agupubs.onlinelibrary.wiley.com/doi/abs/10.1029/2020GL091733` (e2020GL091733 2020GL091733) doi: https://doi.org/10.1029/2020GL091733

Joughin, I., Tulaczyk, S., Bamber, J. L., Blankenship, D., Holt, J. W., Scambos, T.,

& Vaughan, D. G. (2009). Basal conditions for pine island and thwaites glaciers, west antarctica, determined using satellite and airborne data. *Journal of Glaciology*, *55*(190), 245–257. doi: 10.3189/002214309788608705

Marsh, R., Ivchenko, V. O., Skliris, N., Alderson, S., Bigg, G. R., Madec, G., ... Zalesny, V. B. (2015). Nemo–icb (v1.0): interactive icebergs in the nemo ocean model globally configured at eddy-permitting resolution. *Geoscientific Model Development*, *8*(5), 1547–1562. Retrieved from https://gmd.copernicus.org/articles/8/1547/2015/ doi: 10.5194/gmd-8-1547-2015

Mathiot, P., Jenkins, A., Harris, C., & Madec, G. (2017). Explicit representation and parametrised impacts of under ice shelf seas in the z^* coordinate ocean model nemo 3.6. *Geoscientific Model Development*, *10*(7), 2849–2874. Retrieved from https://gmd.copernicus.org/articles/10/2849/2017/ doi: 10.5194/gmd-10-2849-2017

Mathiot, P., & Jourdain, N. C. (2023). High-end projections of southern ocean warming and antarctic ice shelf melting in conditions typical of the end of the 23$^{\text{rd}}$ century. *EGUsphere*, *2023*, 1–27. Retrieved from https://egusphere.copernicus.org/preprints/2023/egusphere-2023-1606/ doi: 10.5194/egusphere-2023-1606

Mouginot, J., Rignot, E., Bjørk, A. A., van den Broeke, M., Millan, R., Morlighem, M., ... Wood, M. (2019, May). Forty-six years of Greenland Ice Sheet mass balance from 1972 to 2018. *Proceedings of the National Academy of Sciences*, *116*(19), 9239–9244. Retrieved 2022-05-31, from https://pnas.org/doi/full/10.1073/pnas.1904242116 doi: 10.1073/pnas.1904242116

Rignot, E., Jacobs, S., Mouginot, J., & Scheuchl, B. (2013). Ice-shelf melting around antarctica. *Science*, *341*(6143), 266-270. Retrieved from https://www.science

.org/doi/abs/10.1126/science.1235798 doi: 10.1126/science.1235798

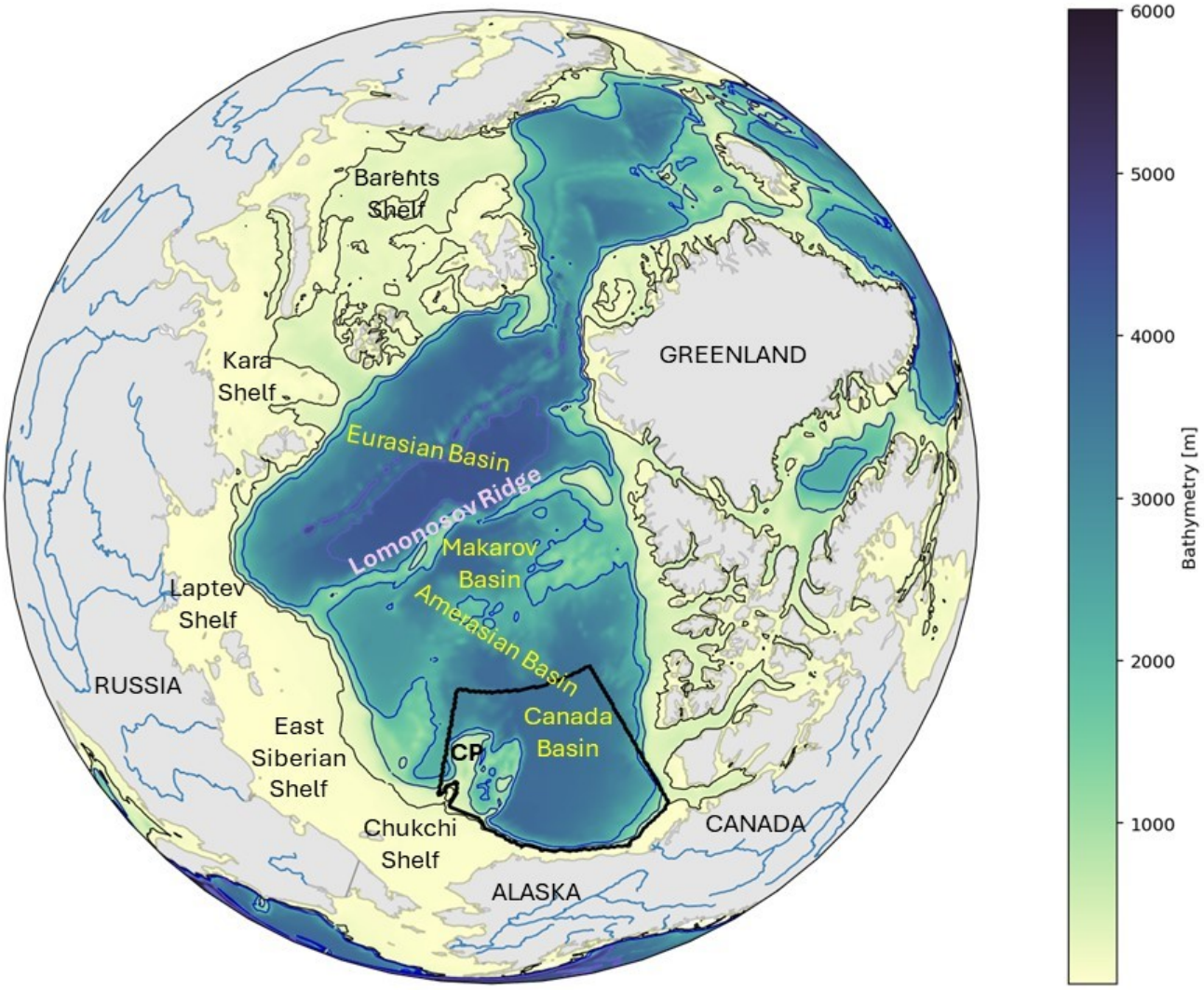

Figure S1. Bathymetric map of the Arctic Ocean in meters. The contours lines delineate the isobaths 200 m, 1000 m, 2000 m, and 4000 m. The Beaufort gyre region box used in this study is contoured in black. The Arctic Ocean is composed of two deep basins on each side of the Lomonosov ridge, the Eurasian Basin and the Amerasian Basin. The Amerasian Basin comprises the Canada Basin and the Makarov Basin. CP is the Chukchi Plateau. The names of the shelves of the Eurasian side are also indicated.

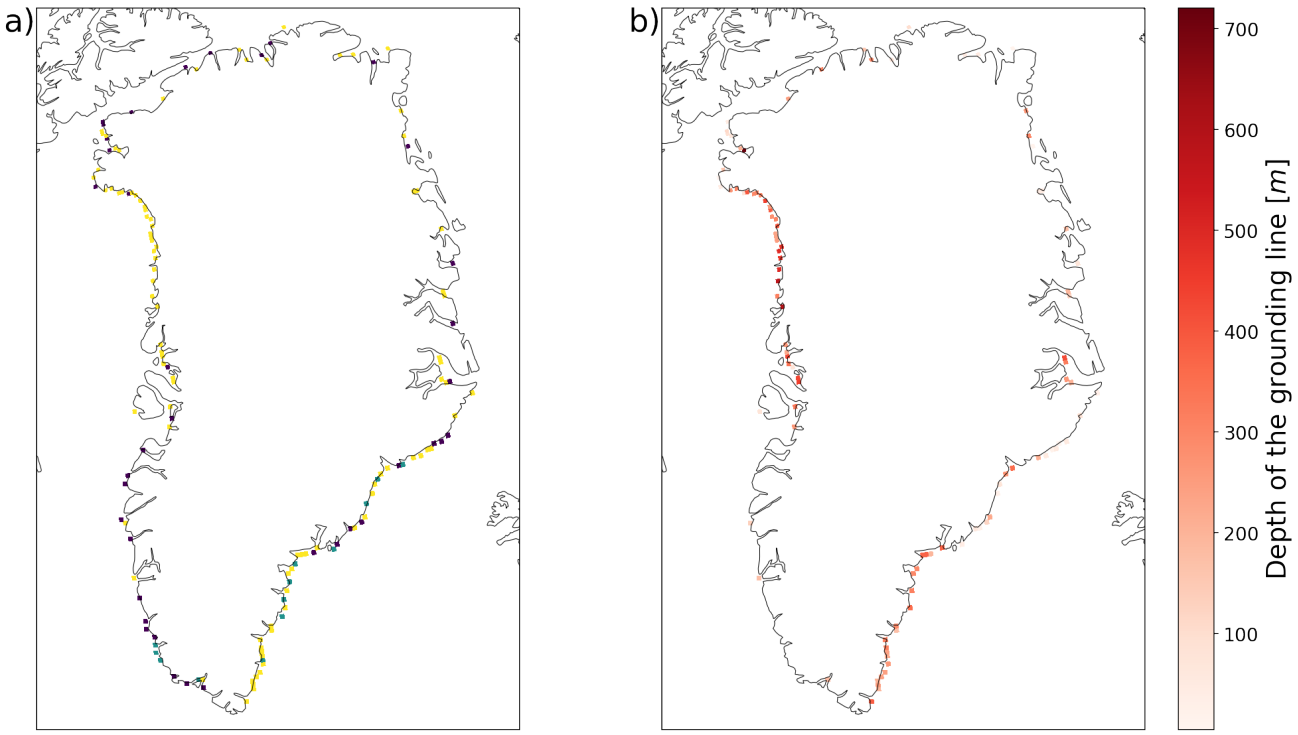

Figure S2. (a) Map of the locations of the freshwater discharge from Greenland forced as surface runoffs only (dark purple dots), as both surface runoff and ice shelf melting (green dots) and as surface runoff, ice shelf melting and iceberg calving (yellow dots). (b) Depth of the grounding line of the Greenland ice sheet marine terminating glaciers.

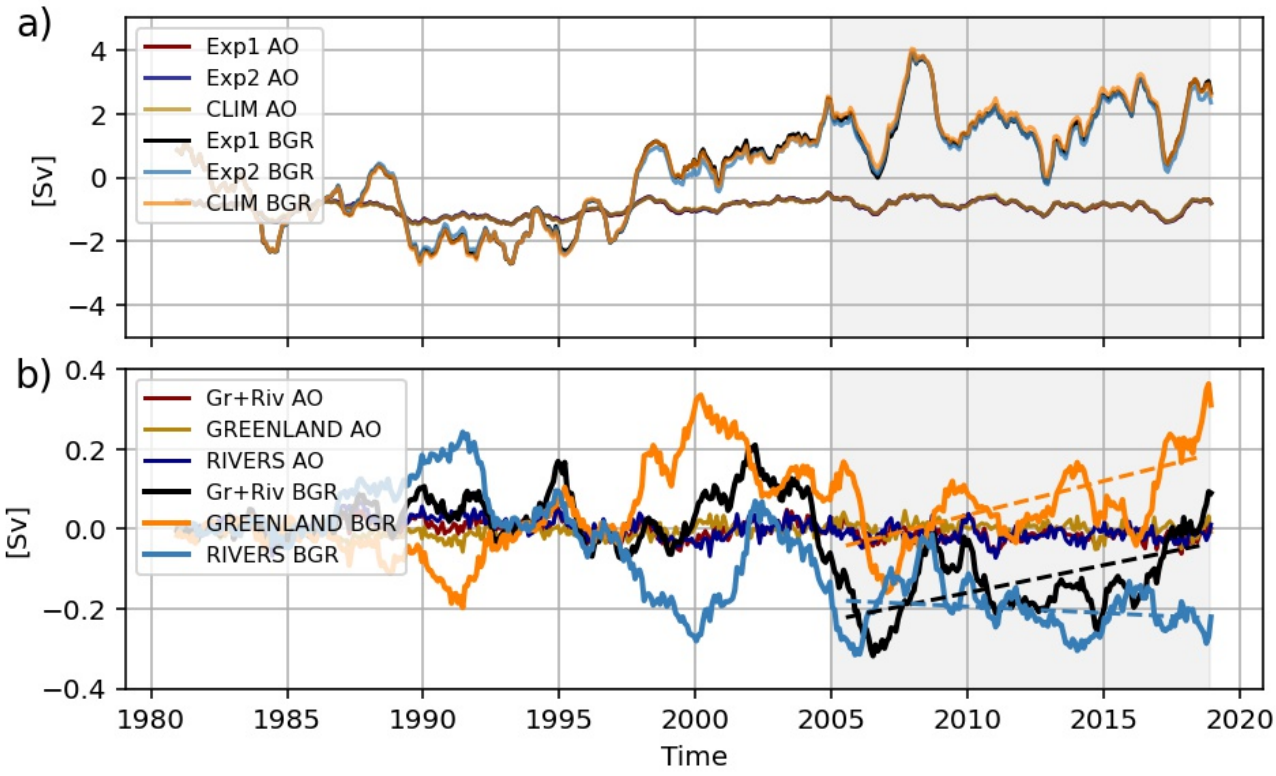

Figure S3. (a) Exp1, exp2, and CLIM barotropic stream function averaged in the BGR box and the Arctic Ocean. (b) Gr+Riv, GREENLAND, and RIVERS barotropic stream function averaged in the BGR box and the Arctic Ocean.

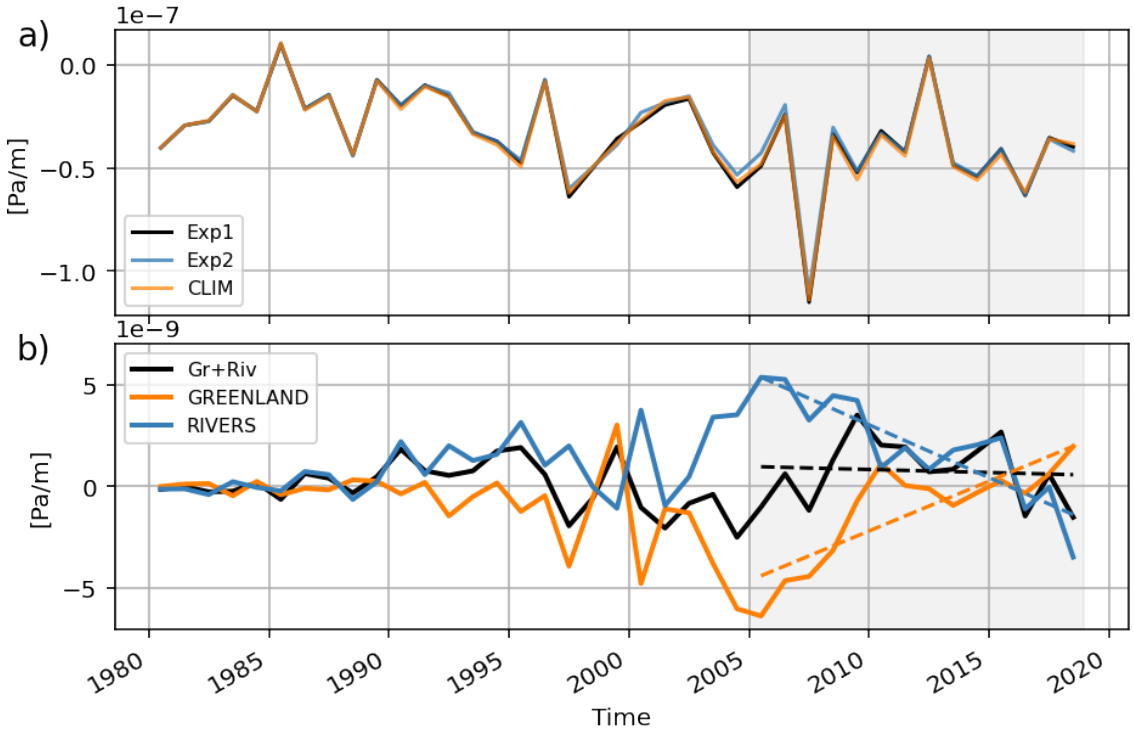

Figure S4. The BGR box wind stress curl perceived by the ocean of (a) exp1, exp2, and CLIM and of (b) Gr+Riv, GREENLAND, and RIVERS.

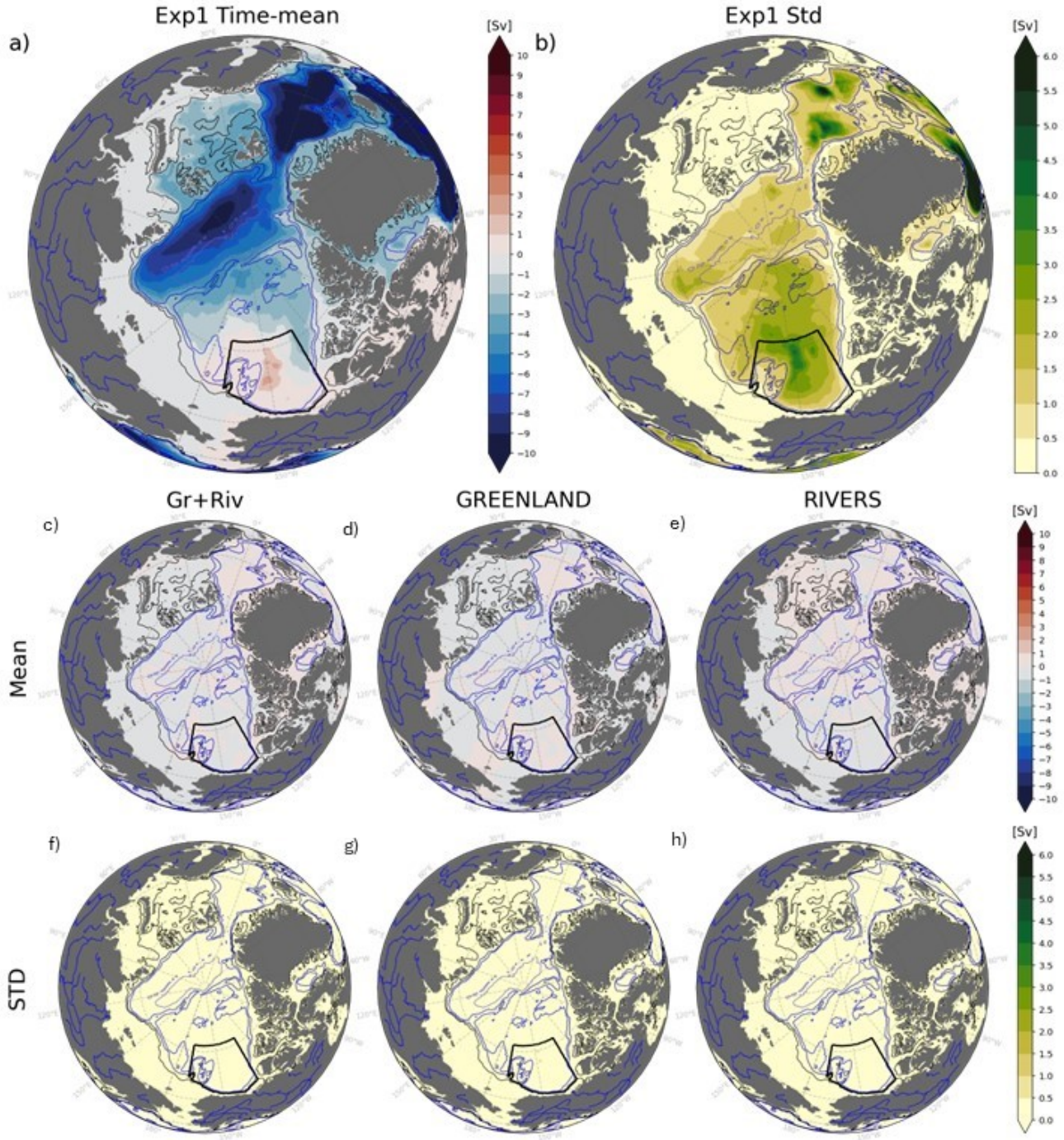

Figure S5. (a) Map of the time-mean of the barotropic stream function of exp1 over 1980-2018. (b) Map of the standard deviation of the barotropic stream function of exp1 over 1980-2018. (c-e) Map of the time-mean of the barotropic stream function of Gr+Riv, GREENLAND, and RIVERS over 1980-2018. (f-h) Map of the standard deviation of the barotropic stream function of Gr+Riv, GREENLAND, and RIVERS over 1980-2018.

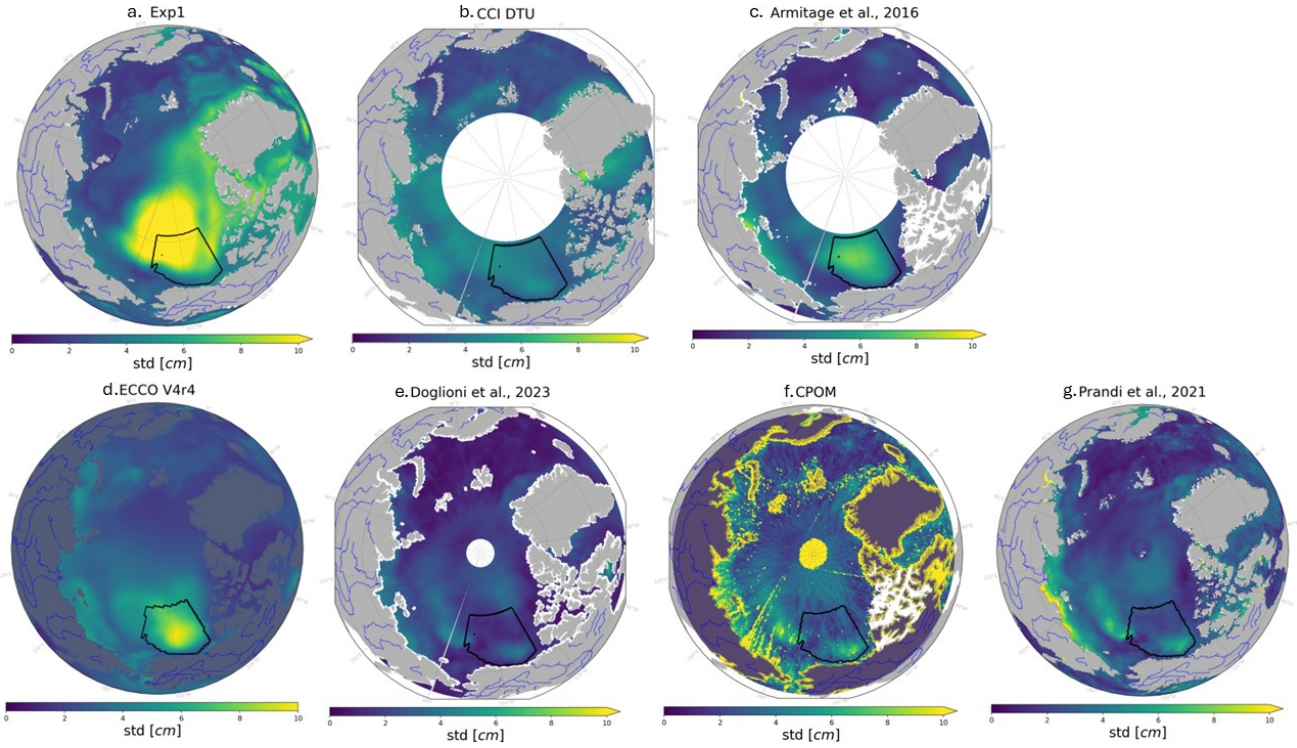

Figure S6. Standard deviation maps computed over the full time period of each dataset: (a) exp1 over 1980-2018, (b) CCI DTU over 1993-2017, (c) Armitage et al., (2016) over 2003-2014, (d) ECCO V4r4 over 1992-2017, (e) Doglioni et al. (2021), over 2011-2018, (f) CPOM over 2011-2018, and (g) Prandi et al., (2021) over 2011-2018.

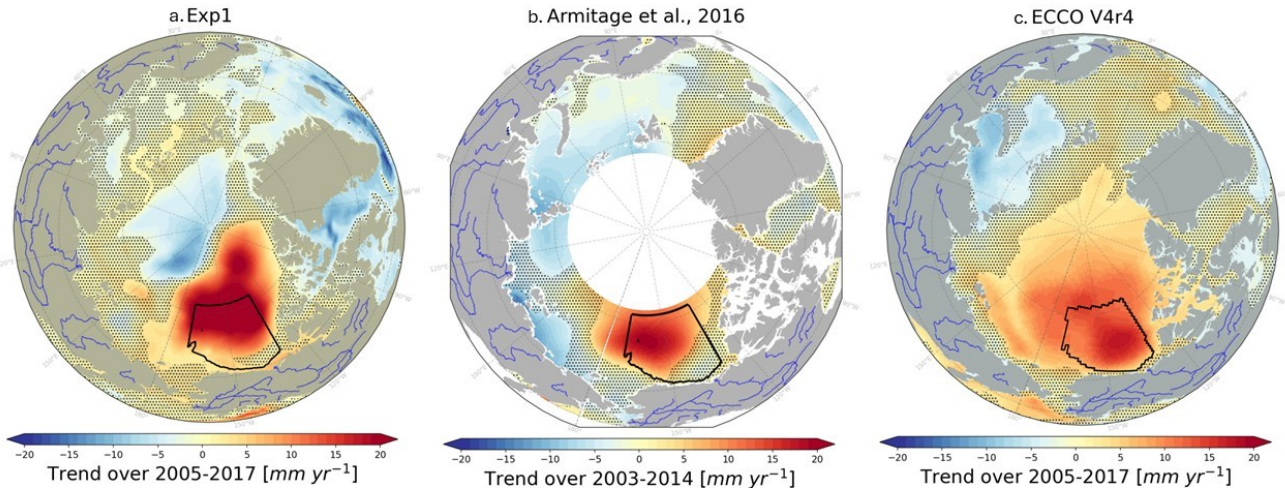

Figure S7. Trend maps computed (a) over 2005-2017 for exp1, (b) over 2003-2014 for Armitage et al., (2016), and (c) over 2005-2017 for ECCO V4r4.

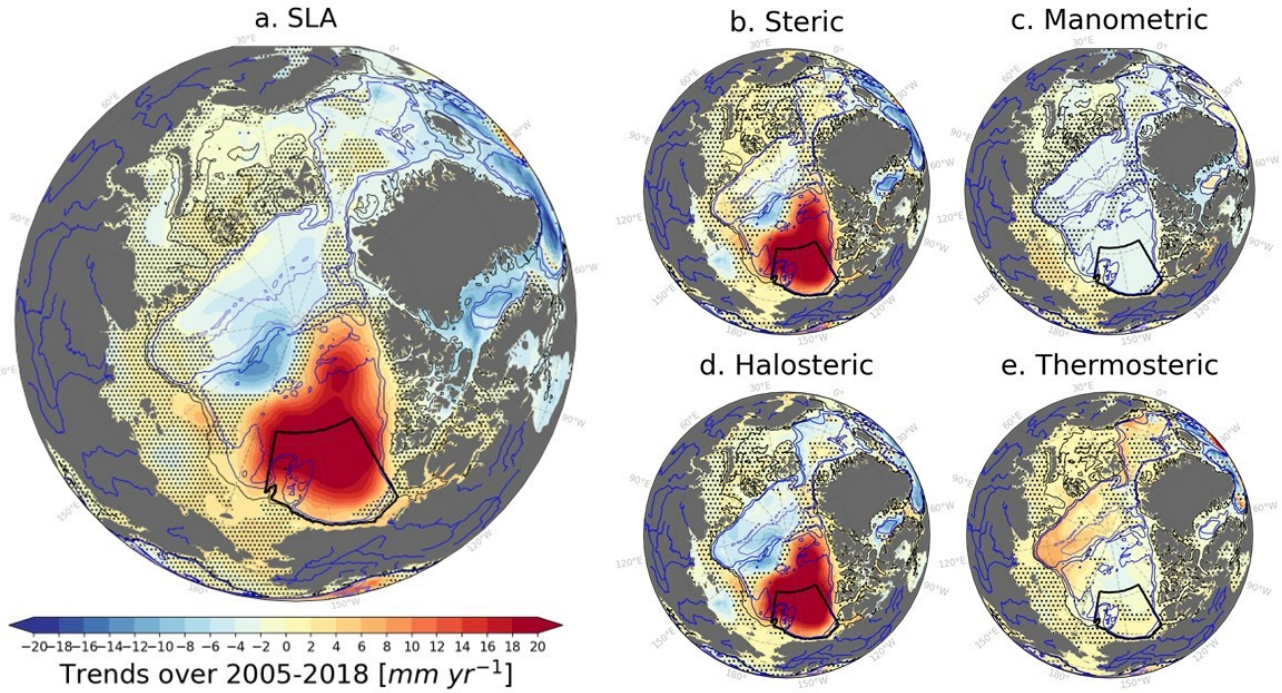

Figure S8. As Fig.3 of the article for exp1: Trends maps over 2005-2018 (a) of SLA, (b) of the full-depth steric sea level, (c) of the full-depth manometric sea level, (d) of the full-depth halosteric sea level, and (e) of the full-depth thermosteric sea level. The black contour is the BGR box. Bathymetry is contoured at 200 m, 1 000 m, 2 000 m, and 4 000 m. Gray stippling indicates the areas where the trends are statistically insignificant below the 90% confidence level using Wald Test with t-distribution.

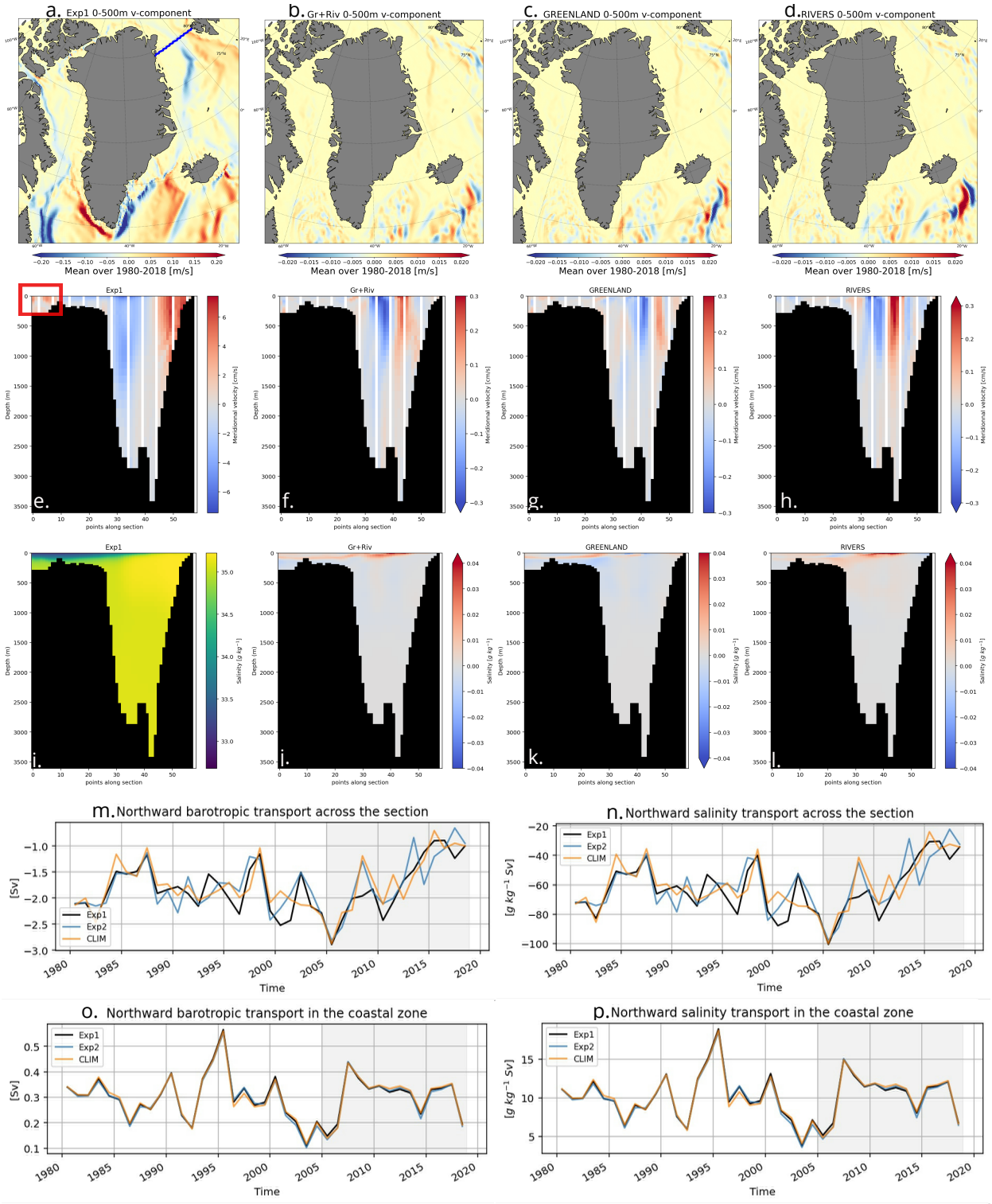

Figure S9. Map of the Meridional velocity component averaged over 0-500 m in exp1 (a) and in Gr+Riv, GREENLAND, and RIVERS (b-d). Blue and red indicate southward and northward velocities respectively. Meridional velocity component along the section indicated in blue in (a) in exp1 (e) and in Gr+Riv, GREENLAND, and RIVERS (f-h). (i-l) is the same as (e-h) for salinity. Northward barotropic transport across the section (positive to the North) in exp1, exp2, and CLIM (m). (n) is the same as (m) for salinity transport. (o-p) are the same as (m-n) for transport across the section in the coastal zone indicated by the red box in (e).

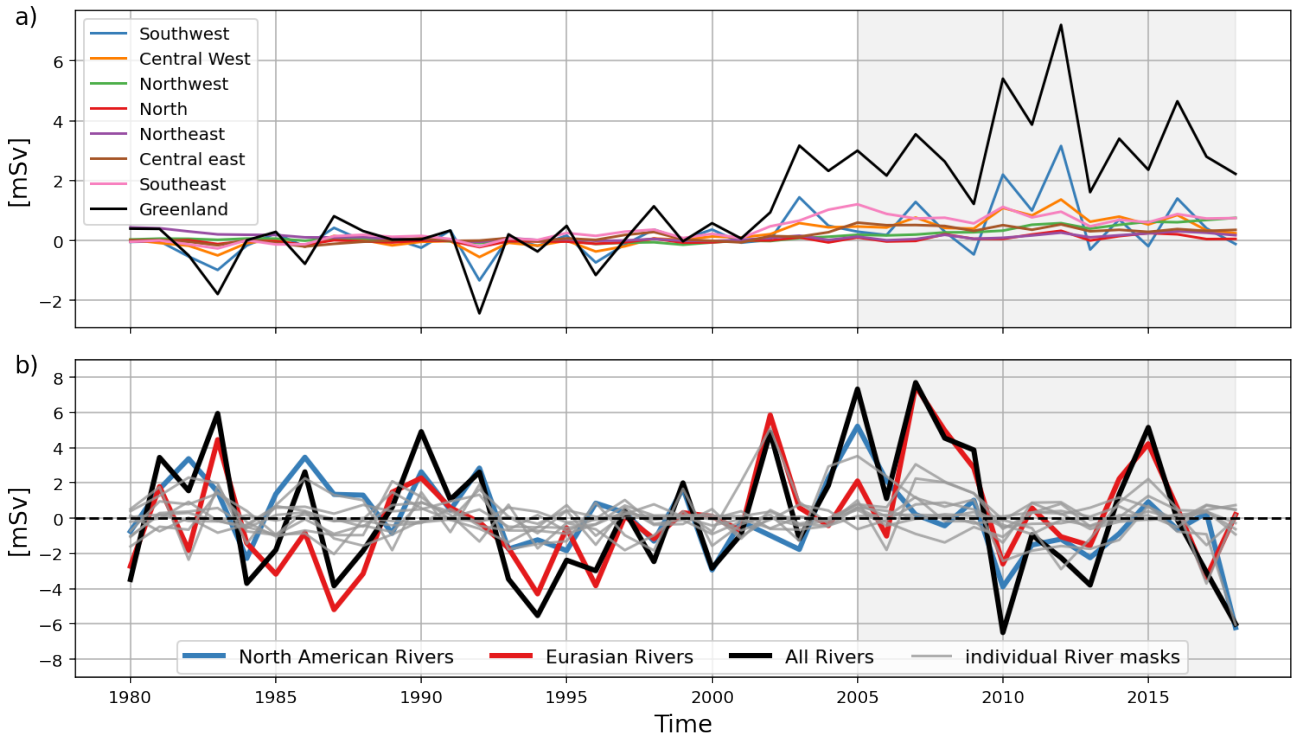

Figure S10. (a) Time series of the annual GREENLAND freshwater discharge by region (colored curves) and for the whole ice sheet (black curve). (b) Time series of the annual RIVERS freshwater flux by region (grey curves), for the pan-Arctic rivers (black curve), the North American Rivers – defined as the masks "Chukchi Sea", "Baffin Bay", "Beaufort Sea", and "CAA" as shown in Fig. 7 – (blue curve), and for the Eurasian rivers -defined as the masks "East Siberian Sea", "Laptev Sea", "Kara Sea", "Barents Sea", and "Norwegian Sea" (red curve).

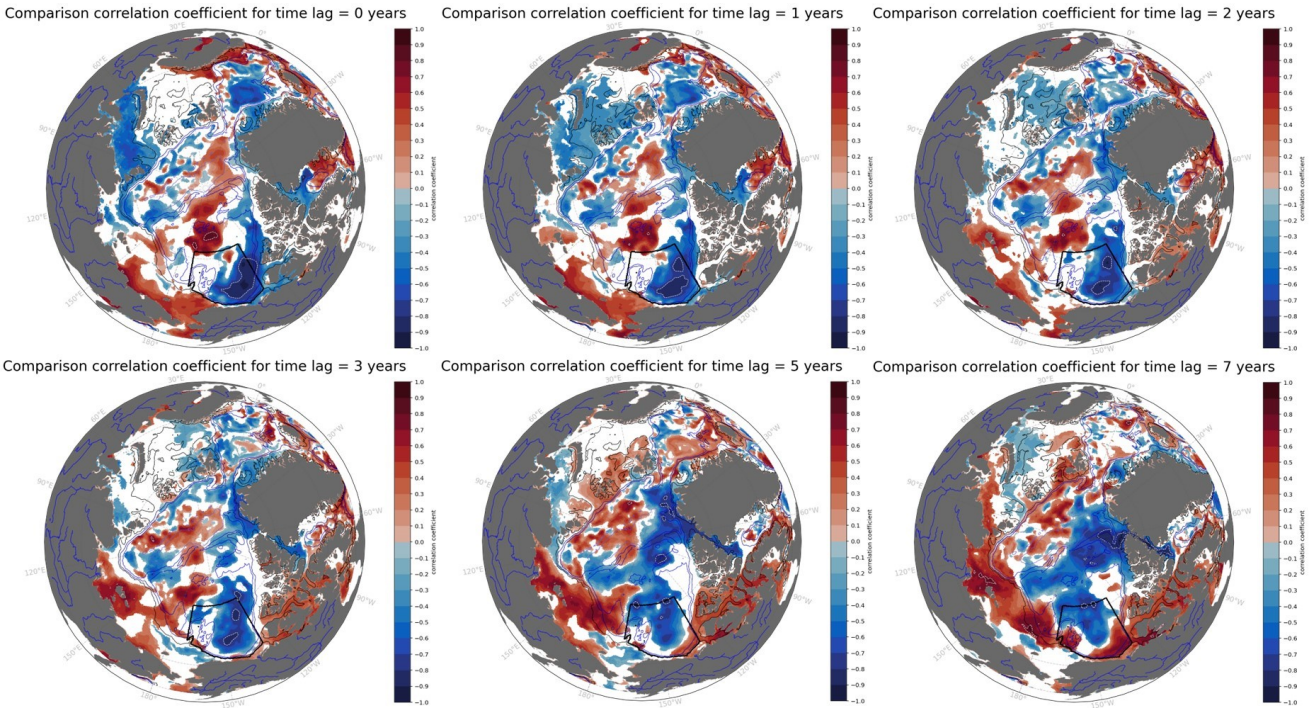

Figure S11. These maps are obtained by doing the mean between the GREENLAND and RIVERS time-lagged correlations maps when they are of the same sign. The white dotted contours highlight the 0.8 correlation line. The white areas of the maps denoted regions where GREENLAND and RIVERS time-lagged correlations are not of the same sign. The time-lagged correlations are computed between the full column mean salinity changes at each grid point in the Arctic Ocean and the time series of SLA in the BGR box over 2005-2018. A lag of 7 years means that the reference time series is compared to the salinity changes of the period 1998-2011.